

Monte Carlo sensitivity analysis of vehicle suspension energy harvesting in frequency domain



Mohamed A.A. Abdelkareem^{a,b,*}, Abdelrahman B.M. Eldaly^{c,d,1}, Mohamed Kamal Ahmed Ali^{a,b}, Ismail M. Youssef^b, Lin Xu^{a,*}

^aSchool of Automotive Engineering, Wuhan University of Technology, Wuhan 430070, China

^bAutomotive and Tractors Engineering Department, Faculty of Engineering, Minia University, El-Minia 61111, Egypt

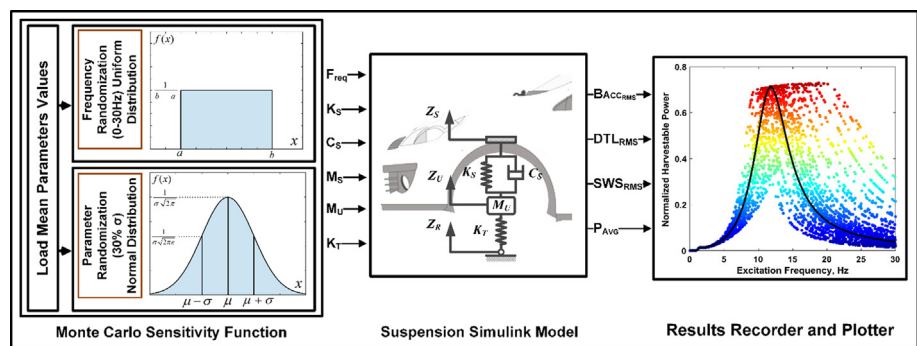
^cDepartment of Electrical Engineering, City University of Hong Kong, Kowloon, Hong Kong

^dDepartment of Communication and Electronics, Faculty of Engineering, Minia University, Minia 61111, Egypt

HIGHLIGHTS

- Frequency based Monte Carlo sensitivity of the harvestable power and vehicle dynamics.
- A widely broadened harvestable power is obtainable terms of higher excitation amplitudes.
- The harvestable energy highly correlated to the damping rate and the tire stiffness.
- The harvestable power responded weakly to the stiffness and the body and wheel masses.

GRAPHICAL ABSTRACT



ARTICLE INFO

Article history:

Received 28 August 2019

Revised 23 January 2020

Accepted 20 February 2020

Available online 22 February 2020

Keywords:

Energy harvesting
Monte Carlo sensitivity
Frequency bandwidth
Automobile suspension
Vehicle dynamics
Vibrations

ABSTRACT

Regenerative shock absorbers (RSAs) have still not entered production lines despite the promising potentials in energy efficiency and emission reduction. Vibration energy harvesting from vehicle dampers has been replicating the dynamics of passive viscous dampers. An accurate frequency-based analysis of the harvestable energy and dynamics for vehicle suspensions under typical operating conditions is essentially needed for designing functional Vibratory Regenerative Dampers (VRDs). This paper proposes frequency-based parametrical bandwidth sensitivity analyses of both the vehicular suspension dynamics and energy harvesting potentiality in accordance with the Monte Carlo sensitivity simulations. This provides insights into which suspension parameter could highly broaden the harvestable power magnitude, which contributes positively to conceptualizing an efficient design of a wide broad-banded energy harvesting damper leading to improved harvesting efficiencies in different road conditions. The conducted sensitivity analysis included the change in both frequency and amplitude bandwidth of the dissipative damping power, body acceleration, dynamic tire load, and suspension deflection. During the sensitivity simulations, a 2-DOFs (degrees-of-freedom) quarter-car model is considered, being excited by harmonic excitations. The selected suspension parameters were normally randomized according to the Gaussian probability distribution based on their nominal values and a 30% SD (standard deviation) with respect to the uniformly randomized excitation frequency. The results inferred higher sensitivity change in the harvestable power bandwidth versus the excitation parameters, damping rate, and tire properties.

Peer review under responsibility of Cairo University.

* Corresponding authors at: School of Automotive Engineering, Wuhan University of Technology, Wuhan 430070, China.

E-mail addresses: mohamed.a.ali@mu.edu.eg (M.A.A. Abdelkareem), xulin508@whut.edu.cn (L. Xu).

¹ M.A.A. Abdelkareem and Abdelrahman B.M. Eldaly equally contributed to this work.

<https://doi.org/10.1016/j.jare.2020.02.012>

2090-1232/© 2020 THE AUTHORS. Published by Elsevier BV on behalf of Cairo University.

This is an open access article under the CC BY-NC-ND license (<http://creativecommons.org/licenses/by-nc-nd/4.0/>).

Conversely, the harvestable power hardly broadened with respect to the body and wheel masses and the spring stiffness.

© 2020 THE AUTHORS. Published by Elsevier BV on behalf of Cairo University. This is an open access article under the CC BY-NC-ND license (<http://creativecommons.org/licenses/by-nc-nd/4.0/>).

Introduction

Motivation

Nowadays, with increasing concern about energy shortage [1], energy harvesting has become a research trend as the harvestable power can be used to power smart sensing applications and self-powered actuators. Large-scale vibration sources such as automobiles presented considerable harvestable power potentiality, such as the dissipated kinetic energy of the vehicular damping events [2–4]. In automobiles, harvesting the dissipated kinetic energy during the damping events could provide fuel saving by 2–10% of the total automobile fueling [5], as indicated in Fig. 1. Interestingly, off-road vehicles, heavy trucks, and those vehicles working in harsh driving conditions infer higher fuel-saving up to 6%, which is related to higher vibration intensity levels referring to more power content to be harvested [6,7]. It is interestingly reported that nearly 13 million dollars per year could be saved when the kinetic energy of the damping events of the Wal-Mart trucks is harvested [8]. In another reported study, using the vibratory energy harvesting dampers into 10% of the Canadian light vehicles could save 8.2 million liters of gasoline a year [9]. This could further result in a reduction of 43.2 kilotons of greenhouse gas emissions. Considering the average gasoline prices in Canada, which is 0.93\$ per liter, nearly 7.6 million dollars a year could be saved if the vibratory damping power is harvested from 10% of the Canadian light vehicles. The harvested electricity during the damping events can be either stored or used to power automotive electrical equipment or power active or semi-active car dampers to enhance the driving comfort and vehicle dynamics.

Prior work

To regenerate the kinetic energy dissipated during vehicle damping events, there are mainly two kinds of vibration-based energy harvesters, which are the electromagnetic mechanized harvesters and piezoelectric harvesters. The piezoelectric harvesters are costly and could mainly be used for small-scale vibration energy harvesting applications [10,11]. The electromagnetic mechanized harvestable dampers can regenerate the kinetic energy during damping events either from linear motion through the linear electromagnetic harvesters [12–14] or from rotary motion through the rotary electromagnetic harvestable dampers based on a linear-to-rotary motion converter [3,15–17]. In the linear-to-rotary motion converters or also known as power-take-off mechanisms, the up and down perpendicular motion could be converted to unidirectional rotation through either a mechanical transmission or a hydraulic transmission integrated with motion rectifiers [18,19]. Motion rectifiers ensure one-way rotation to drive a rotary generator and generate electricity with the highest possible efficiency [20–22].

Given the literature, several quantification analyses were published regarding the experimental and theoretical estimation of the kinetic energy dissipation during suspension damping events. The authors in [23] carried out several real on-field driving tests regarding the estimation of the harvestable damping power for different driving speeds and with respect to real road sections, including city-roads with and without speed bumps. During their on-field experimentations using a HAVAL H8 SUV, the average

power dissipation per damper can be in a range of 10–90 W for a speed range of 20–50 km/h and road section without speed bumps while a kinetic energy in a range of 40–140 W was estimated for the same speed range and a road section with a speed bump. In another quantification analysis of the harvestable power by Zuo and Zhang [24], the on-road driving results showed that the overall harvestable power during the damping events of a passenger car ranged from 100 to 400 W when driving on smooth and rough roads with a 96.5 km/h speed. Zhao et al. [25] designed a piezoelectric energy harvester to assess the energy harvesting potential from vehicle suspensions under random and pulse road excitations. The results reported that a harvestable power of 18.83 W was obtained at 30 km/h and random road of Class B, while, in case of the pulse road, the maximum respective harvestable power was 102.24 W. Based on a comprehensive conflict analysis, Abdelkareem et al. [26] addressed the trade-off between the harvestable power and truck dynamics for a verified full trailed truck model with respect not only to the bounce road input but also including the roll road excitation mode. Furthermore, a quantification analysis of the overall harvestable power was conducted, and the damping power dissipated by the tractor, trailer, and cabin were estimated as 0.968, 0.894, and 0.186 kW, respectively.

In an investigation by Riese et al. [27], the potential energy harvesting dissipated by shock absorbers of compact-class passenger cars was addressed, including the pitch movement due to the acceleration of the vehicle. During this study, parameter analysis was considered to study the influence of different vehicle factors on harvestable energy. The results reported that a higher amount of the harvestable vehicular energy is highly correlated to rough roads and with medium to high vehicle speed ranges. The Monte Carlo sensitivity simulation was recently introduced in terms of the parameter sensitivity analysis of the vibratory energy harvesters based automobile suspension [28,29]. Taghavifar and Rakheja [28] presented a parametric analysis of the potential of energy harvesting considering a 4-wheeled generic three-dimensional full-car

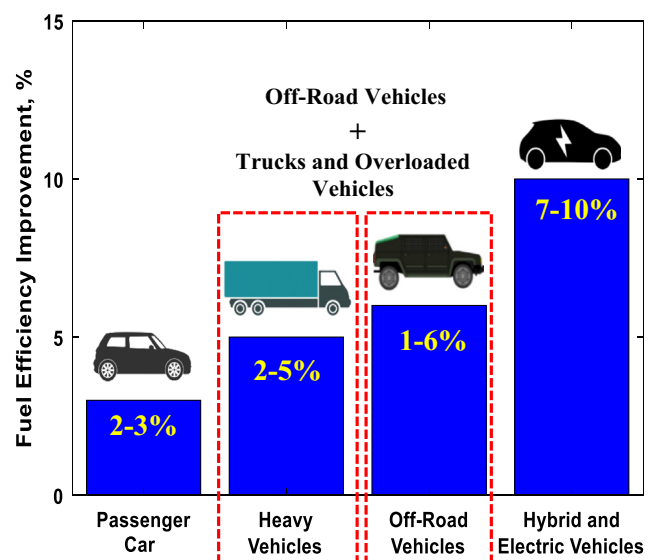


Fig. 1. Fuel saving potentials as a result of harvesting the kinetic energy during vehicle damping events. (Reproduced and drawn with permission from Ref. [5]).

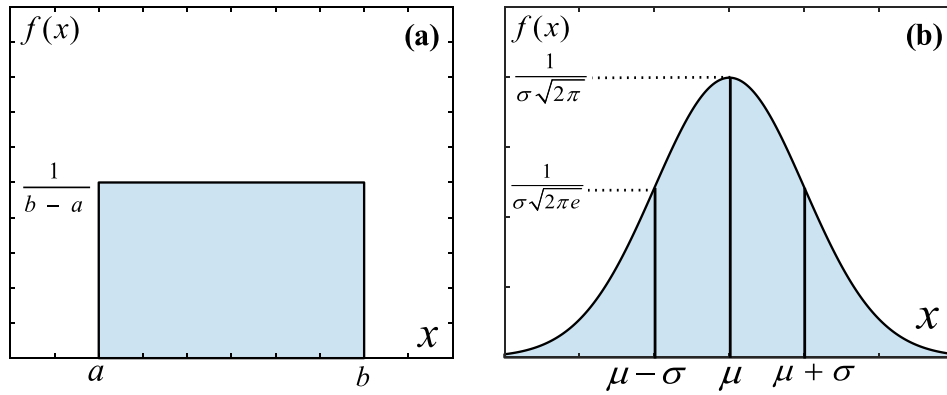


Fig. 2. Probability distribution function; (a) uniform distribution of the excitation frequency, (b) normal Gaussian distribution of the suspension parameters.

suspension model and on-road classes defined in ISO 8608:1995. The performed analyses were done based on the Monte Carlo simulations regarding the analysis of the harvestable power content and its correlation to the vehicle acceleration levels for different suspension and driving conditions. Summing up their sensitivity results, the root-mean-square (RMS) harvestable power results indicated larger magnitudes of the damping energy dissipation in terms of rough terrains than smooth road profiles, which thereby suggested considerable harvestable power content are available in case of commercial vehicles on off-road terrains. Zhang et al. [29,30], with respect to the Monte Carlo sensitivity simulations, conducted a comparative investigation for both the direct and indirect drive vibratory energy harvesters in terms of regenerative shock absorbers to assessed their energy harvesting abilities. It is inferred that the Monte Carlo sensitivity approach interestingly presented its remarkable effectiveness regarding the analysis of the system parameters influences, especially in terms of the frequency-based sensitivity analysis.

Contribution

It is noteworthy that researchers and manufacturers are still investigating an efficient broad-banded energy harvesting vehicle damper considering the random nature of road vibrations. Thus, it is needed to develop an efficient energy harvesting damper that could adequately capture useful electricity during both the low-frequency and high-frequency banded scenarios. Most of the conducted studies mainly addressed how the driving speed and road roughness affect the harvestable power, while the effects of the suspension model parameters have been introduced in only a few research studies [28]. The reported investigations have been mostly limited to time-domain parametric analysis of the harvestable power during the damping events, which not precisely characterize the harvestable energy behavior in terms of the frequency bandwidth. Thus, comprehensive bandwidth and sensitivity analyses are needed, including both the sensitivity of the harvestable power bandwidth (magnitude and frequency bandwidth) considering the effects of the design and operating factors.

This study fundamentally provides an investigation of both the frequency and amplitude bandwidth sensitivity of the damping energy-harvesting potentiality and quarter suspension dynamics, including ride quality and road holding. The frequency-based parametrical bandwidth sensitivity was performed based on the Monte Carlo simulations. The Monte Carlo based sensitiveness included the damping rate, spring stiffness, tire stiffness, sprung mass, unsprung mass, and the harmonic excitation amplitude. During the sensitivity simulations, the mean harvestable power is calculated while the RMS values of the bounce acceleration, suspension

Table 1

Vehicle quarter suspension parameters.

Parameter	Value	Parameter	Value
Sprung mass (M_S)	350 kg	Unsprung mass (M_U)	40 kg
Spring stiffness (K_S)	25 kN/m	Tire stiffness (K_T)	200 kN/m
Damping coefficient (C_S)	1500 N.s/m	Sine wave amplitude	0.01 m

deflection, and the dynamic tire load are considered with respect to the uniformly randomized frequency ranged between 0 and 30 Hz. This paper also aimed to provide insights into which suspension parameter could highly broaden the vehicular damping harvestable power magnitude. This contributes positively regarding conceptualizing an efficient design of a wide broad-banded energy harvesting damper, which leads to improved harvesting efficiencies in different road conditions. The simulation results are also analyzed to highlight the bandwidth change in both the peak-amplitude and resonant frequency bandwidth of the ride comfort and road holding.

Simulation setup

This section presents the parametrical bandwidth sensitivity simulations, including the Monte Carlo function design and the investigated vehicular suspension dynamics. Furthermore, both the quarter suspension parameters and the simulation flow are indicated. Fundamentally, Monte Carlo simulations investigate the uncertainties in a probabilistic way by constructing the models of possible results through the substitution of a range of values considering a probability distribution for each model parameter [29–31]. During the simulation trails, the values of the selected parameters are sampled randomly based on the input probability distributions. Input probability distributions can take different forms, including uniform, normal, and triangular. Noteworthy, the Monte Carlo sensitivity method enables mimicking real road profile conditions in frequency domains [28]. Each set of samples is called iteration, and the resulting outcome from that sample is recorded during simulation runs.

Monte Carlo parametrical bandwidth sensitivity function

During the sensitivity simulations, a 2-DOFs quarter suspension model is considered, which is excited by harmonic excitations. With regards to the bandwidth sensitivity analysis, based on the Monte Carlo simulations, the excitation frequency was randomly sampled in the range of 0–30 Hz with respect to the uniform probability distribution (Fig. 2a) according to the probability density function given in Eq. (1). Otherwise, the residual suspension

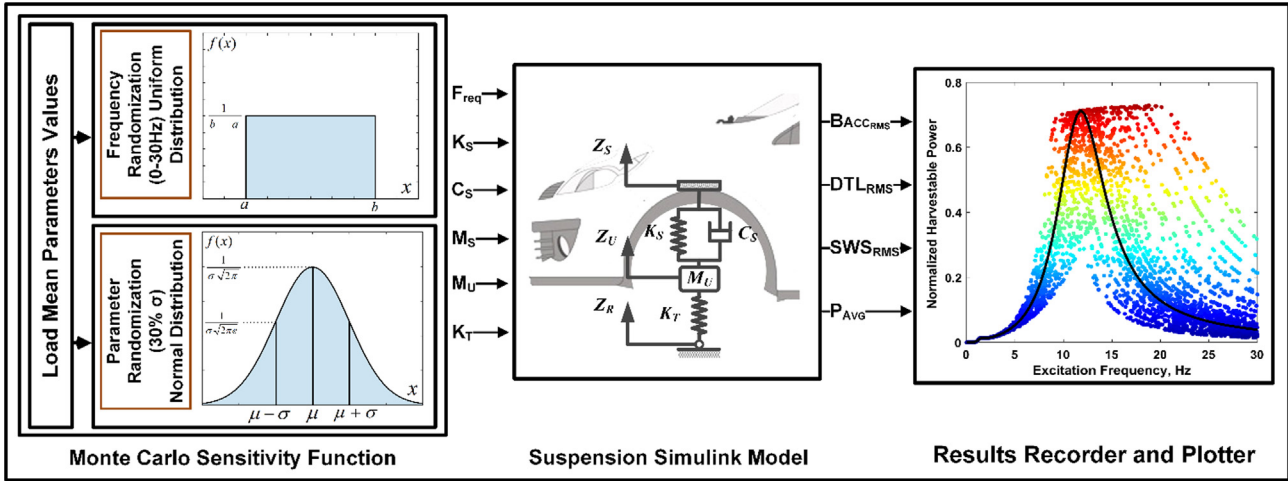


Fig. 3. Flow diagram of the Monte Carlo frequency based parametrical sensitivity simulations.

parameters were randomized based on the normal probability distribution, also known as the Gaussian probability distribution, with respect to their nominal values and a standard deviation of 30% (Fig. 2b). The Gaussian probability density function is given in Eq. (2). The bandwidth sensitivity analysis included spring stiffness, damping rate, body and wheel masses, tire stiffness, and the harmonic excitation amplitude. Noteworthy, the parameters randomization sampling was 80 points per parameter, and the sampling of the excitation frequency was also 80 points.

$$f(x) = \frac{1}{b-a} \text{ for } a \leq x \leq b \quad (1)$$

where $f(x)$ is the probability density function (PDF), a is the minimum value of x , b is the maximum value of x , and x is the random variable.

$$f(x) = \frac{1}{\sigma\sqrt{2\pi}} e^{-\frac{(x-\mu)^2}{2\sigma^2}} \text{ for } -\infty < x < \infty \quad (2)$$

where $f(x)$ is the probability density function, μ is parameter mean value, σ is the standard deviation, and x is a random variable.

Vehicular harvestable power and suspension dynamics criteria

The Monte Carlo based bandwidth sensitivity analysis included the vehicular damping harvestable power and suspension dynamics. The bandwidth sensitivity simulations were performed based on a 2-DOFs quarter suspension model. The investigated car dynamics included the bounce mass acceleration, suspension deflection, and the dynamic tire load (DTL). The proposed suspension dynamics are usually considered to investigate both the car ride quality and ground holding [32–34]. In automobiles, the kinetic energy dissipated during the damping events can be either evaluated in terms of the average power or the RMS power value [35,36]. Basically, the instantaneous harvestable damping power is computed by multiplying the squared dynamic suspension velocity by the damping coefficient in terms of the time domain form [23]. In this paper, during the sensitivity simulations, the average damping harvestable power is considered, which is calculated as shown in Eq. (3). Otherwise, the RMS of the sprung mass acceleration, suspension working span, and the dynamic tire load are calculated in Eqs. (4)–(6), respectively.

$$P_{avg} = C_s \left(\frac{1}{n} * \sum_{i=1}^n (\dot{Z}_B(t) - \dot{Z}_w(t))^2 \right) \quad (3)$$

$$Acc_{RMS} = \sqrt{\frac{1}{T} \int_0^T \|\ddot{Z}_B(t)\|^2 dt} \quad (4)$$

$$SWS_{RMS} = \sqrt{\frac{1}{T} \int_0^T \|(Z_B(t) - Z_w(t))\|^2 dt} \quad (5)$$

$$DTL_{RMS} = K_T \sqrt{\frac{1}{T} \int_0^T \|(Z_w(t) - Z_R(t))\|^2 dt} \quad (6)$$

where P_{avg} denotes the mean value of the damping harvestable power. Acc_{RMS} , SWS_{RMS} and DTL_{RMS} represent the suspension dynamics criteria in terms of the RMS of the body bounce acceleration, suspension deflection, and dynamic tire load, respectively. $\ddot{Z}_B(t)$ donates for the time domain vehicle body acceleration. Whereas, $Z_B(t)$, $Z_w(t)$ and $Z_R(t)$ donates for the sprung mass, unsprung mass, and road time domain displacements, respectively. C_s represents the damping rate of the passive damper while K_T donates for the tire equivalent stiffness.

During the simulations, the bandwidth sensitivity simulation results were recorded in terms of the normalized and dimensionless responses to precisely illustrate the sensitivity of both the frequency and amplitude bandwidth to the proposed parametric analysis. In this manner, both the vehicle dynamics and energy harvesting responses were normalized by their reference nominal values recorded using the nominal values of the suspension parameters listed in Table 1. Given the suspension dynamics responses, the normalized RMS trends of the body acceleration ($N_{Acc_{RMS}}$), suspension deflection ($N_{SWS_{RMS}}$), and dynamic tire load ($N_{DTL_{RMS}}$) are calculated as illustrated in Eqs. (7)–(9). While the normalized average damping harvestable power ($N_{P_{Avg}}$) is calculated according to Eq. (10).

$$N_{Acc_{RMS}} = \frac{Acc_{RMS}(i)}{Acc_{RMS_{Ref}}} \quad (7)$$

$$N_{SWS_{RMS}} = \frac{SWS_{RMS}(i)}{SWS_{RMS_{Ref}}} \quad (8)$$

$$N_{DTL_{RMS}} = \frac{DTL_{RMS}(i)}{DTL_{RMS_{Ref}}} \quad (9)$$

$$N_{P_{Avg}} = \frac{P_{Avg}(i)}{P_{Avg_{Ref}}} \quad (10)$$

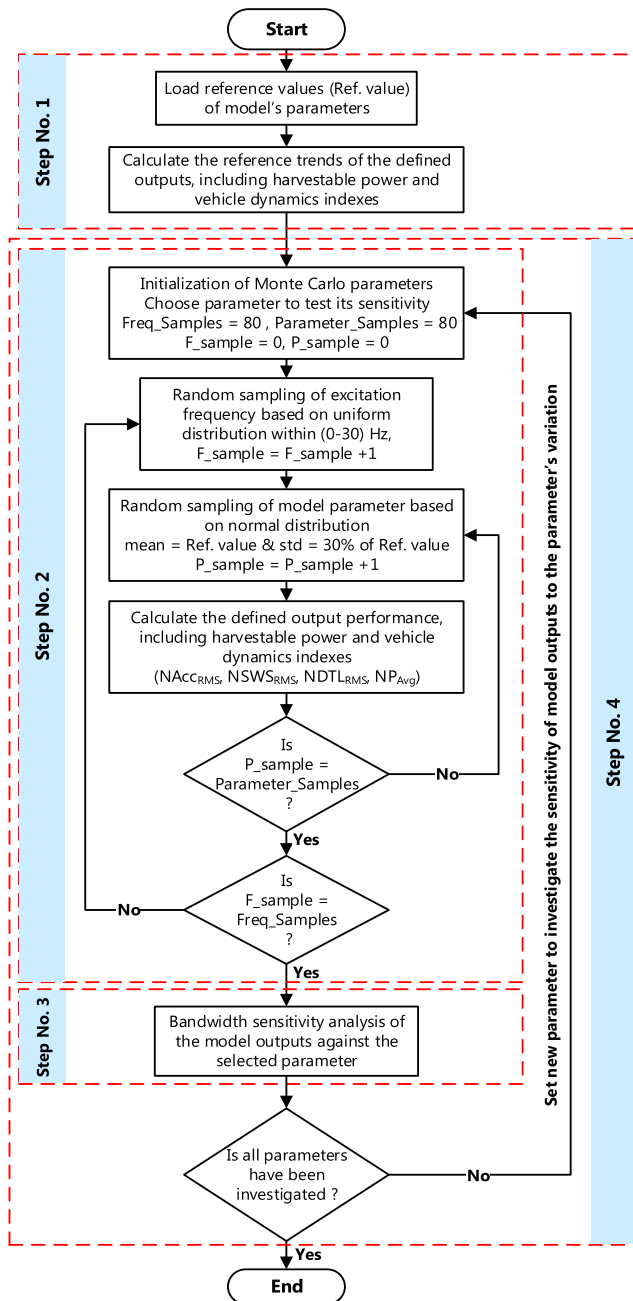


Fig. 4. Schematic diagram of the proposed simulation methodology during the sensitivity simulations.

where $NACC_{RMS}$, $NSWS_{RMS}$, and $NDTL_{RMS}$ stands for the normalized RMS body acceleration, suspension working space, and dynamic tire load, respectively. NP_{Avg} donates the normalized average damping harvestable power. ACC_{RMSRef} , SWS_{RMSRef} , DTL_{RMSRef} , and P_{AvgRef} donate the reference nominal recorded values of the body acceleration, suspension deflection, dynamic tire load, and harvestable power, respectively. The aforementioned normalized indices were computed with respect to the randomly generated values of the frequency and suspension parameters for each iteration (i).

Parameters and simulation flow

The Monte Carlo based bandwidth sensitivity simulation was performed based on the simulation infographic shown in Fig. 3. Table 1 lists the nominal parameters used in the implemented

Monte Carlo parametrical bandwidth sensitivity function. During the simulations, the excitation frequency is randomized based on uniformly probability distribution function between 0 and 30 Hz, as shown in Fig. 2a. Otherwise, the remaining investigated suspension parameters are randomly sampled based on the Gaussian probability distribution (Fig. 2b) with respect to their nominal values listed in Table 1 and a 30% standard deviation. The parametrical bandwidth sensitivity included the suspension stiffness, damping rate, unsprung and sprung masses, tire equivalent stiffness, and the excitation amplitude. These sensitivity simulations were executed using the MATLAB/Simulink[®] platform with respect to the Runge-Kutta solver, simulation time of 5 s, and 0.001 sampling time. In Fig. 4, the detailed schematic diagram of the proposed bandwidth sensitivity simulation's methodology is illustrated. The major simulation steps are summarized as follows:

The model reference parameters are loaded and thereafter the reference trends of the harvestable power and suspension dynamics (body acceleration, suspension deflection and dynamic tire load) are calculated.

The Monte Carlo simulation parameters are initialized. Thereafter, based on the uniform probability distribution, the excitation frequency was randomly sampled with a sampling of 80 samples. The investigated model parameter is then sampled based on the normal probability distribution with respect to the reference parameter value and a standard deviation of 30%. Thereafter, the harvestable power and vehicle dynamics indexes are calculated and stored.

The bandwidth sensitivity analyses are conducted to elaborate and emphasize the sensitivity correlation of the harvestable power and suspension dynamics indexes.

A new parameter is picked to investigate its sensitivity and correlation versus the harvestable power and suspension dynamics.

Results and discussions

Extensive simulations were carried out regarding the frequency and amplitude bandwidth sensitivity analysis of the damping energy-harvesting potentiality and the quarter vehicle dynamics, including the sprung-mass acceleration, dynamic tire force, and suspension deflection.

Harvestable power and suspension dynamics sensitivity versus suspension parameters

Fig. 4 illustrates the normalized damping power potentiality, sprung-mass acceleration, dynamic tire force, and the suspension deflection with respect to a randomized input frequency and a 30% SD randomized damping rate. Obviously, in terms of the peak-amplitude bandwidth, the randomized damping rate showed a noticeable influence on the energy-harvesting, dynamic tire load, and suspension deflection, as regarded in Fig. 4a, c, and d. In Fig. 4b, it is inferred that there is no noticeable effect of the damping coefficient on the peak-amplitude of the sprung mass acceleration. Given the frequency bandwidth of the response's peak-amplitude, the suspension damping implied fixed frequency broadband of the energy-harvesting potentiality, body acceleration, dynamic tire load, and the suspension deflection. This confirms that the damping rate variation contributed toward extending the peak-amplitude band of these responses without any significant effect on the frequency broadband. Concludingly, the amplitude bandwidth sensitivity of the aforementioned responses clearly correlated to the damping rate variation, unlike the frequency bandwidth sensitivity of their peak-amplitude

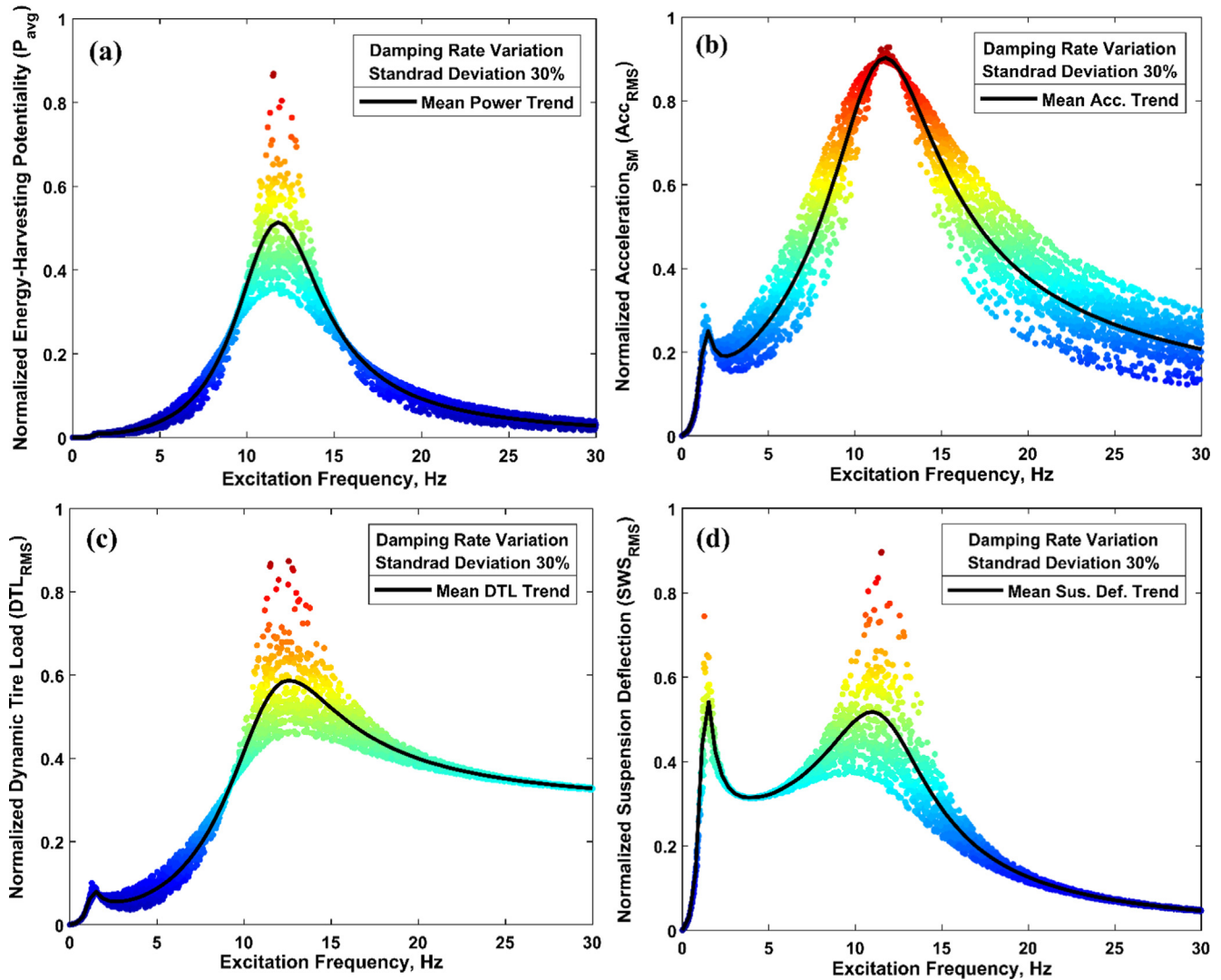


Fig. 5. Normalized responses of the damping power potentiality, sprung-mass acceleration, dynamic tire force and the suspension deflection with respect to the 30% SD randomized damping rate.

which is changed hardly with regards to the 30% SD randomized damping coefficient.

Fig. 5 presents the normalized trends of the energy-harvesting content and suspension dynamics to reveal both the amplitude and frequency bandwidth sensitivities and the sensitivity change of the resonant frequencies of these responses against a 30% SD randomly sampled spring stiffness. It is inferred from Fig. 5a–d that both the peak-amplitude and resonant frequency bandwidth of the above-mentioned responses are slightly sensitive to the suspension stiffness variation. It is concluded that the sensitiveness of the peak-response-amplitude of the potential power and suspension dynamic responses correlated clearly to the randomly sampled stiffness rates with a 30% SD and a nominal stiffness of 25 kN/m. On the other hand, the response-natural-frequency broadband presented lower sensitivity change to the suspension spring stiffness variation. For example, in Fig. 5b and d, the peak-amplitude bandwidth of the body acceleration and suspension deflection fluctuated slightly around the trend of the modal responses that is originality plotted based on the nominal suspension parameters. Summing up the aforementioned analysis, the sensitivity change of the peak amplitude and resonant frequency bandwidth corresponding to the mentioned responses insignificantly correlated to the spring stiffness variation.

Fig. 6 reveals the normalized energy-harvesting and suspension dynamics corresponding to a randomly sampled tire stiffness (30% SD of a nominal tire stiffness of 200 kN/m) concerning a sampled sine-wave frequency span of 0–30 Hz. In Fig. 6a, looking at the normalized damping energy harvesting trend, it is demonstrated that both the amplitude and frequency bandwidth considerably broadened with a 30% SD randomized tire stiffness. This makes the energy harvesting bandwidth strongly sensitive to the tire characteristics. Similarly, the suspension dynamics responses (sprung-mass acceleration, dynamic tire force, and suspension deflection) demonstrated similar behavior, as revealed in Fig. 6b, c, and d. At higher tire stiffnesses, the tire transfers higher vibration intensity levels to the body mass through the suspension assembly. Accordingly, the broader harvesting-potentiality bandwidth can result in the aggressive and high vibration intensity levels, which is possibly achieved in the case of heavy-duty and off-road vehicles with corresponding higher tire stiffnesses. The tire stiffness sensitivity simulations concluded that the increase of the tire stiffness could broaden both the frequency and amplitude bandwidth of the energy harvesting and suspension dynamic responses.

Fig. 7 displays the bandwidth analysis of the energy harvesting and suspension dynamics with respect to the sprung mass variation (30% SD of a sprung mass of 350 kg), and a randomly sampled

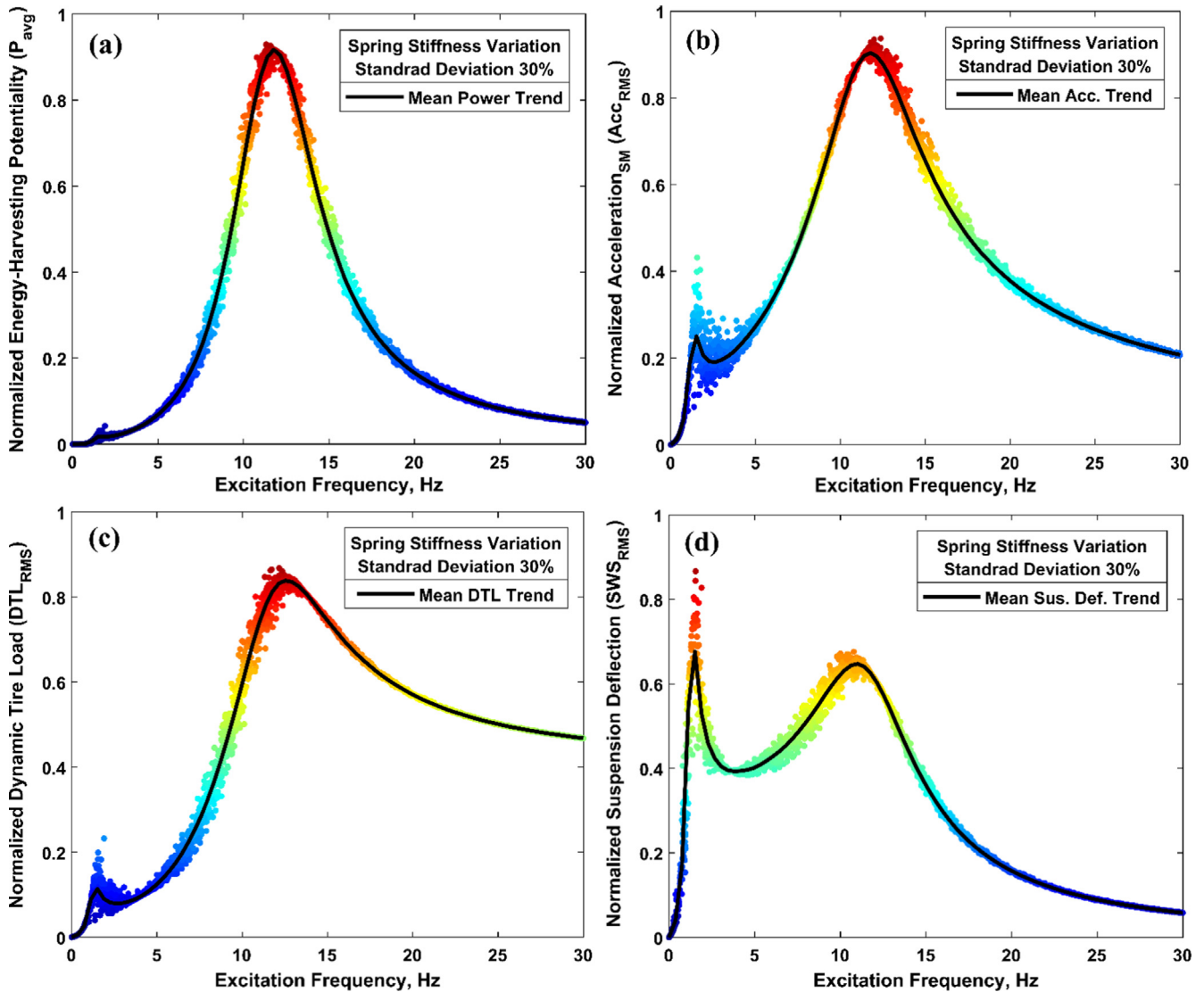


Fig. 6. Normalized responses of the damping power potentiality, sprung-mass acceleration, dynamic tire force and the suspension deflection with respect to the 30% SD randomized spring stiffness.

frequency ranged from 0 to 30 Hz. The potentially harvested power responded weakly to the sprung mass variation, as shown in Fig. 7a, which reveals lower sensitivity change in the energy harvesting bandwidth against the sprung mass parameter. Similar trends are observed for both the dynamic tire load and the suspension deflection, as given in Fig. 7c and d. By contrast, as revealed in Fig. 7b, the body acceleration responded markedly to the variation of the sprung mass showing high sensitivity change in terms of the acceleration amplitude bandwidth. The peak-amplitude acceleration is broadened by 75% approximately with respect to a sprung mass variation with a standard deviation of 30%.

Fig. 8 illustrates the sensitivity correlation between the damping power potentiality, body mass acceleration, dynamic tire force, and the suspension deflection versus the variation of the unsprung mass. The wheel mass was randomly sampled based on a nominal mass value of 40 kg and a 30% standard deviation. Fig. 8a and b inferred that the variation of the wheel mass widely broadened the resonant frequency bandwidth of both the harvestable power and body acceleration while the peak magnitude band hardly responded. This concludes higher sensitivity change in the frequency band of the aforementioned responses, while conversely

lower sensitivity in their magnitude bandwidth is observed. Given the DTL sensitivity results in Fig. 8c, the peak amplitude of the DTL corresponds to the wheel mass resonant frequency is advanced by nearly 16%. In addition, the resonant frequency of the DTL response is shifted from 12.5 Hz at the nominal mass value to 9.8 Hz, showing a 2.7 Hz retard ratio in the resonant frequency with respect to a 30% SD randomly sampled wheel mass. In Fig. 8d, the suspension deflection sensitivity inferred identical attitude for that of the DTL response. This is related to the remarkable impact of the wheel mass on the unsprung mass deflection and thereby affect the ground road holding ability in terms of the dynamic tire force.

The results in Fig. 9 address the bandwidth sensitivity analysis of the harvestable power, ride behavior, and ground holding ability with respect to the excitation amplitude variation. The magnitude bandwidth of the harvestable power, body acceleration, dynamic tire force, and suspension deflection presented a higher correlation with the excitation amplitude. Whereas, the natural resonant frequency bandwidth presented weak sensitivity change with respect to the varied road input magnitude. Increasing the excitation amplitude produces higher and aggressive vibration intensities, which positively contribute to a broad bandwidth of the

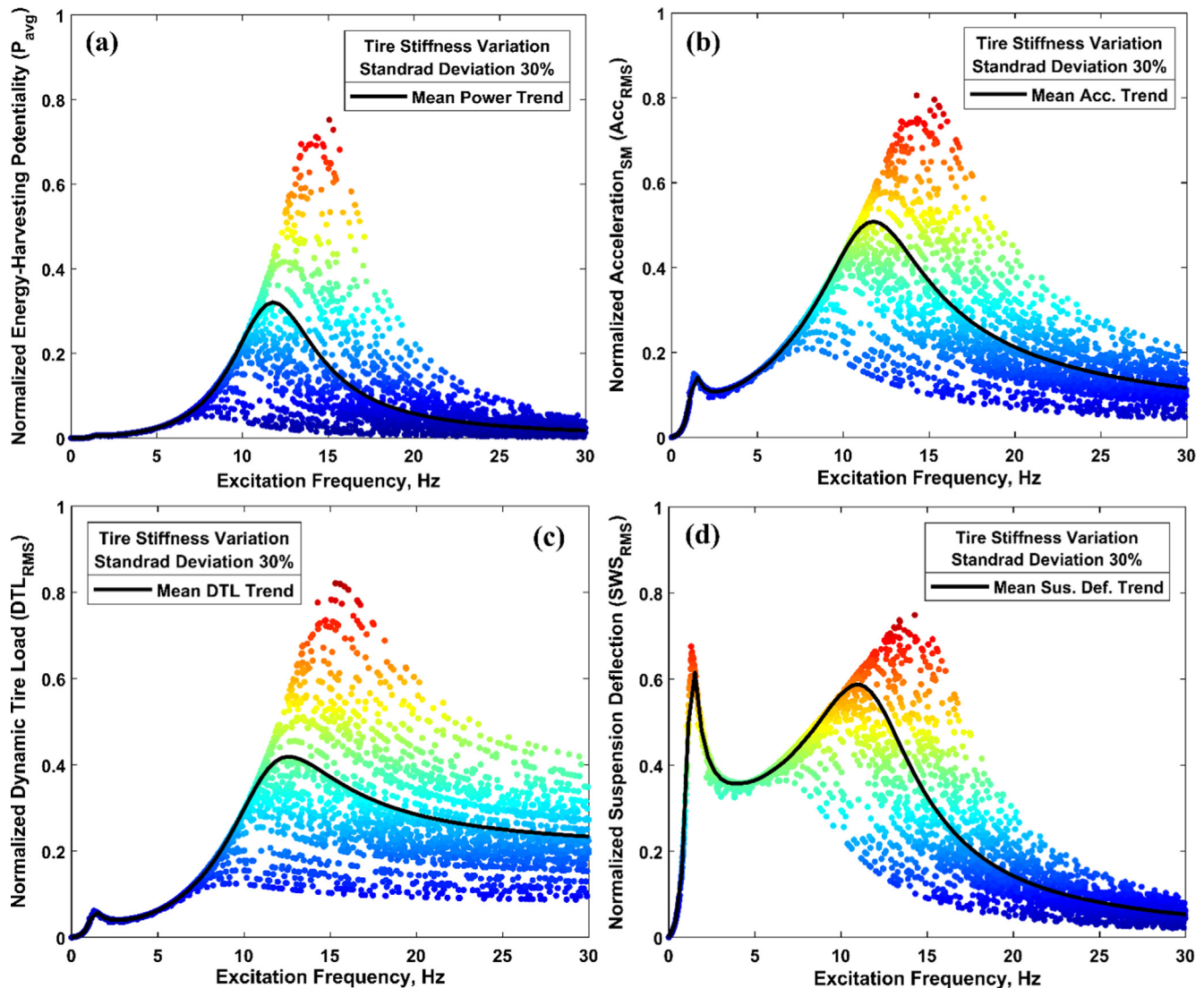


Fig. 7. Normalized responses of the damping power potential, sprung-mass acceleration, dynamic tire force and the suspension deflection with respect to the 30% SD randomized tire stiffness.

harvestable damping power. With a 30% SD randomly sampled excitation amplitude, the peak-magnitudes corresponding to the wheel natural resonant frequency of the aforementioned responses responded remarkably to the increase in the excitation amplitude as inferred in Table 2. The same sensitivity attitude is observed for the peak magnitudes corresponds to the body's natural resonant frequency. Conversely, the natural resonant frequency bandwidth hardly broadened versus the amplitude variation.

According to the recorded results in Table 2, the peak-magnitudes of the potentially harvested damping power located at both the first and the second natural frequencies increased by 140% and 149%, respectively, comparing to the reference case. Remarkably, broader harvesting power bandwidth can be achieved through rough and off-road terrains. This is because of the road magnitude and roughness directly affects the suspension deflection and thereby the content of stored energy in the suspension springs [28]. On the other side, the peak-magnitudes of the body acceleration increased by almost 60% compared to the reference body acceleration computed at the nominal parameters. The first peak-magnitude of the RMS DTL corresponding to the first resonant frequency similarly witnessed an increase of 66%.

Bandwidth analysis of the vehicular damping harvestable power

This section investigates the sensitivity percentage of change of the damping harvestable power magnitude against the randomly sampled model parameters based on their reference values and a 30% SD. During the bandwidth sensitivity simulations, the sensitivity change in both the amplitude and resonant frequency bandwidth of the peak magnitudes of the harvestable power is illustrated.

Fig. 10 reveals a bandwidth analysis of the average harvestable power potentiality versus the variation of suspension model and input parameters. The bandwidth analysis includes both the resonant frequency and amplitude bandwidths of the peak magnitudes of the harvestable power. Furthermore, Table 3 concludes the bandwidth analysis results of the harvestable power magnitude during damping events concerning a 30% SD of the nominal value of suspension parameters. It is evident from Fig. 10a that the damping rate markedly broadened the amplitude band of the harvestable power peak magnitude, but the resonant frequency band revealed almost no change in its bandwidth against the 30% SD randomly sampled damping rate. It can be further inferred from

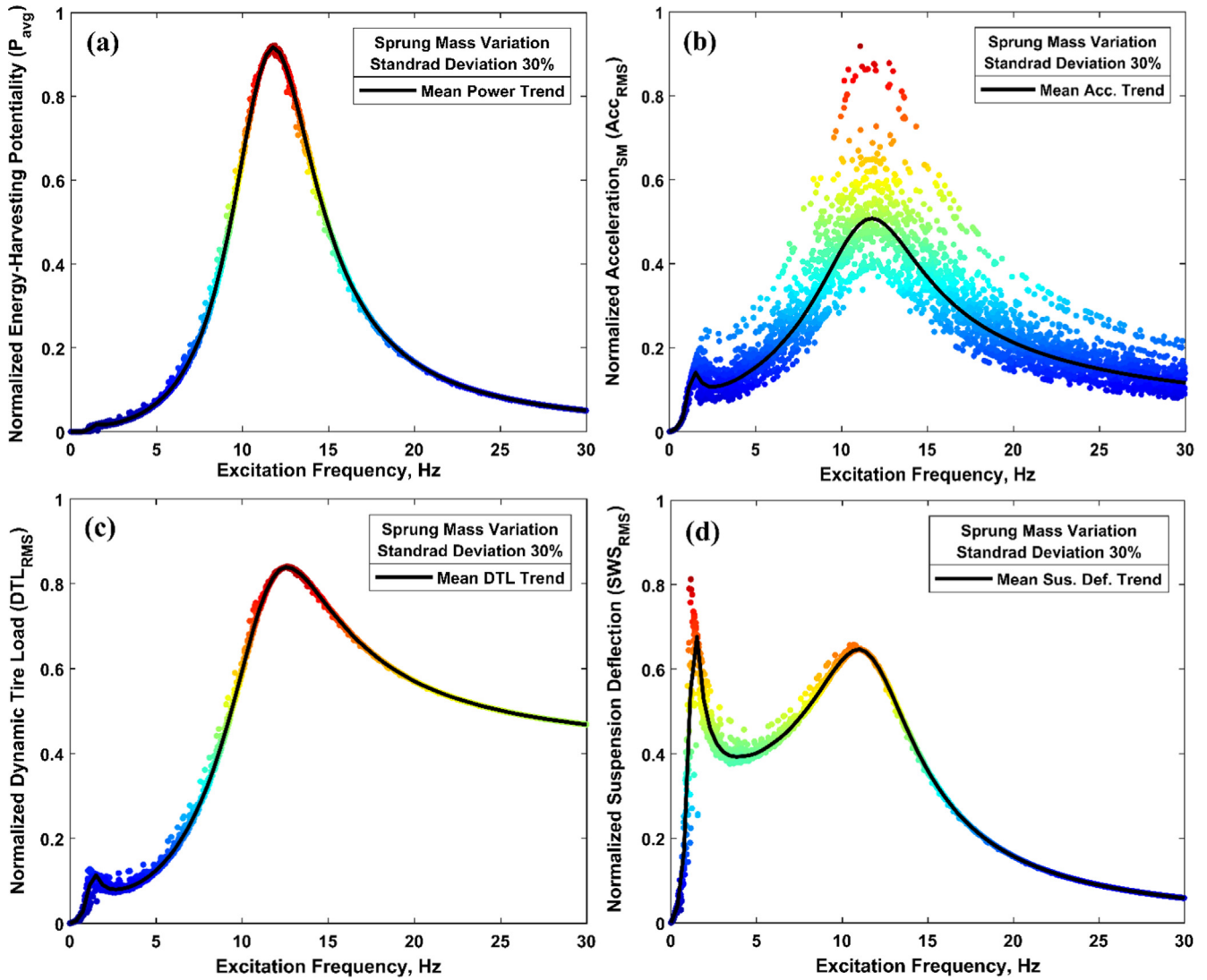


Fig. 8. Normalized responses of the damping power potential, sprung mass acceleration, dynamic tire force and the suspension deflection with respect to the 30% SD randomized sprung mass.

Fig. 10a and Table 3 that the peak-magnitude of the harvestable power corresponding to the wheel mass resonant frequency is increased from 1.28 kW at 11.77 Hz resonant frequency to 2.16 kW at 11.49 Hz showing a 68% broadened magnitude. This is related to the direct correlation between the harvestable damping power and the damping coefficient. In terms of suspension dynamics, the damping rate mainly affects the magnitude of the response without a markable effect on the resonant frequency band. The observed correlations were similarly confirmed in Ref. [26].

It is reported from Fig. 10b and d that both the spring stiffness and the sprung mass parameters barely broadened the bandwidth of the damping harvestable power magnitude. This is due to the weak sensitivity change in the harvestable power magnitude against the slight change in both of the sprung mass and spring stiffness. The correlations and sensitivity change of the harvestable power were similarly confirmed in Ref. [6]. Conversely, as in Fig. 10c, the tire stiffness variation broadened not only the peak-magnitude of the harvestable power but also the resonant frequency but with higher sensitivity change in the amplitude bandwidth than that of the resonant frequency band. The peak-magnitude of the harvestable power is boosted in terms of the

amplitude band by nearly 135%, while its resonant frequency band is broadened from 11.77 Hz at the nominal tire stiffness value (200 kN/m) to 15 Hz showing a 27% forward shift in the peak-magnitude resonant frequency. This is likely due to the markable effect of the tire stiffness on the transmitted vibrations to the suspension system and thereby influences the suspension velocity, which is the main indication for the damping harvestable power trend at constant damping rates.

In Fig. 10e, the unsprung mass variation markedly broadened the resonant frequency bandwidth of the harvestable power peak-magnitude while there is almost no change in the amplitude bandwidth. The resonant frequency is considerably broadened by nearly 71% advance in the peak-magnitude frequency band, as concluded in Table 3. It is noteworthy that the harvestable power magnitude correlated strongly to the 30% SD randomized road amplitude, which indicates higher sensitivity change in the magnitude bandwidth of the harvestable power contrasting the sensitivity change in the resonant frequency bandwidth. Thanks to the aggressive vibration intensity levels, which positively advance the relative suspension velocity and thereby broadened the harvestable power magnitude referring to higher harvestable energy content for rough terrains. In Fig. 10f, the magnitude of the

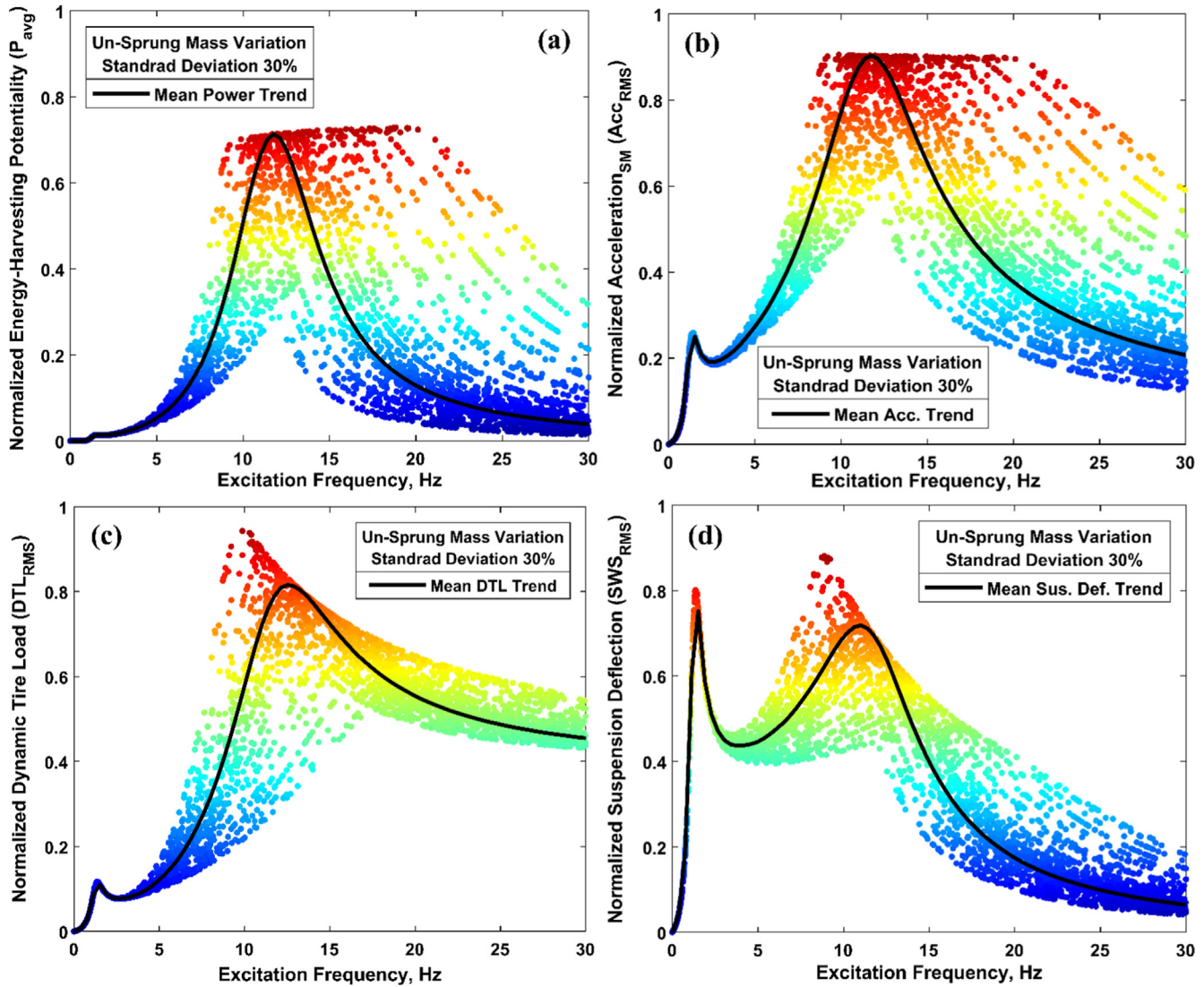


Fig. 9. Normalized responses of the damping power potentiality, sprung-mass acceleration, dynamic tire force and the suspension deflection with respect to the 30% SD randomized unsprung mass.

Table 2
Bandwidth analysis of the harvestable power, sprung-mass acceleration, dynamic tire force and the suspension deflection power with respect to 30% SD of the excitation amplitude.

Response	Bandwidth sensitivity ^a			
	Amplitude bandwidth ^b		Resonant frequency bandwidth ^c	
	1st peak ^d	2nd peak ^e	1st peak	2nd peak
Harvestable power	140%	149%	-8%	-2%
Body acceleration	63%	60%	-8%	-2%
Suspension deflection	43%	59%	-10%	-
Dynamic tire load	66%	59%	-8%	-

^a The maximum percent change in both the peak magnitude the amplitude and resonant frequency bandwidths is considered.

^b The percent change in the amplitude of the main peak-magnitude of the harvestable power above the mean power trend at nominal parameters in considered.

^c The (-) sign refers for the backward shift in the natural resonant frequency.

^d The peak-magnitude corresponding to the body mass resonant frequency.

^e The peak-magnitude corresponding to the wheel mass resonant frequency.

potentially harvested energy has been broadened by nearly 149% versus a 30% SD randomly sampled road amplitude and a nominal amplitude of 0.01 m.

Fig. 11 illustrates the correlation of the instantaneous harvestable power and the corresponding suspension relative velocity

versus the variation of the model parameters highlighting both the high and lower harvestable power content. In Fig. 11a, the instantaneous harvestable power/velocity correlation is given with respect to different damping rates, and the contour plot on both of the x-y and z-y axes reveals the damper velocity/damping rate

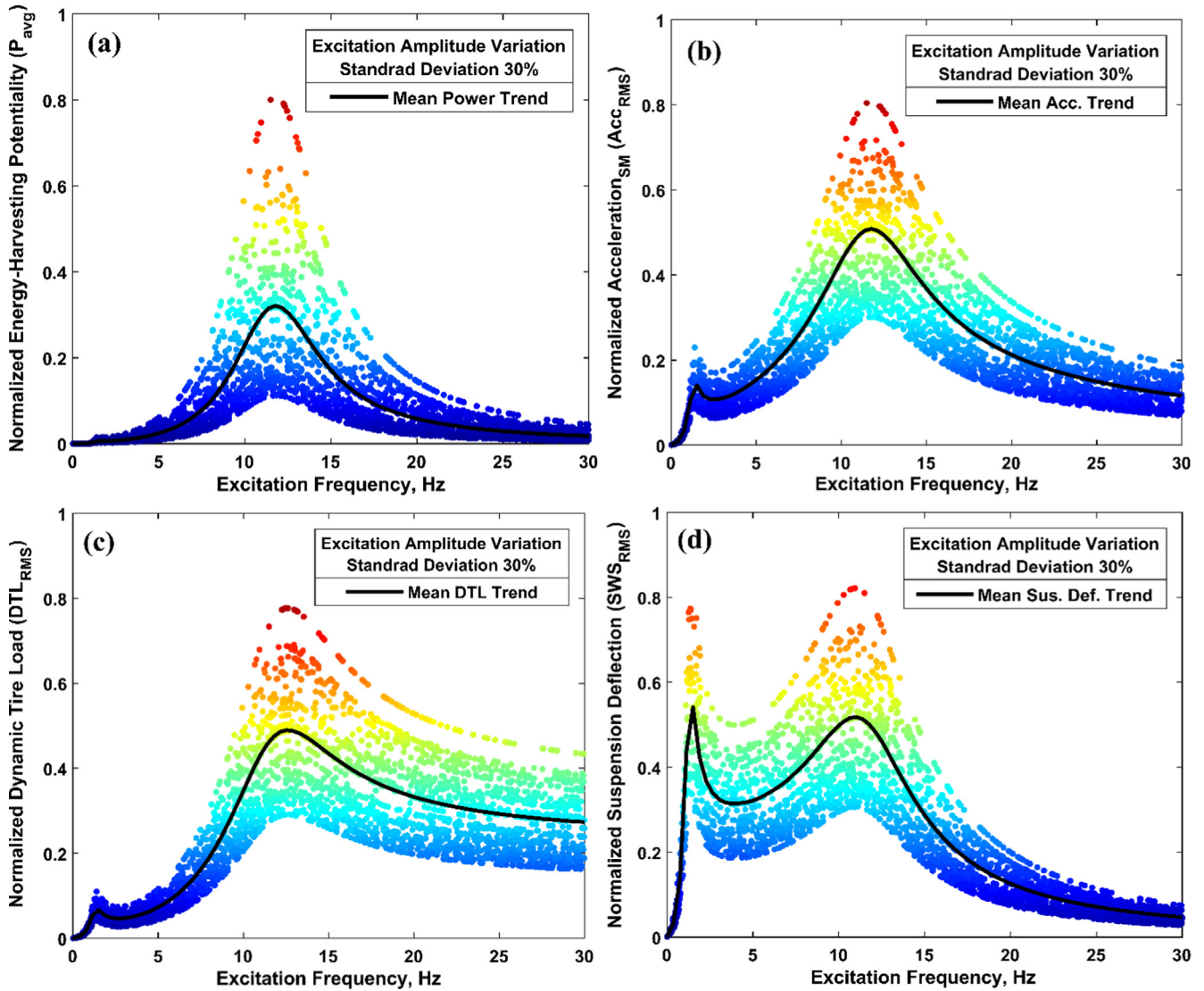


Fig. 10. Normalized responses of the damping power potential, sprung-mass acceleration, dynamic tire force and the suspension deflection with respect to the 30% SD randomized excitation amplitude.

and the harvestable power/velocity correlations. A typical correlation of the instantaneous damping harvestable power and the suspension velocity is plotted as a non-linear cup-curve respecting the

Table 3
Bandwidth analysis harvestable power magnitude during vehicular damping events with respect to 30% SD of the nominal value of suspension parameters.

Response	Nominal value	Harvestable power bandwidth ^a	
		Amplitude bandwidth ^b	Resonant frequency bandwidth ^c
Damping rate, N s/m	1500	68%	-2%
Spring stiffness, kN/m	25	1%	-2%
Tire stiffness, kN/m	200	135%	+27%
Sprung mass, kg	350	-	-
Unsprung mass, kg	45	2%	+71%
Excitation amplitude, m	0.01	149%	-2%

^a The maximum percent change in both the peak magnitude the amplitude and resonant frequency bandwidths is considered.

^b The percent change in the amplitude of the main peak-magnitude of the harvestable power above the mean power trend at nominal parameters is considered.

^c The (+) sign donates for forward shift in the resonant frequency while the (-) sign refers for the backward shift.

compression and rebound events since the power is functioned of the square damping velocity. The higher harvestable power content is related to higher damping velocities and higher damping rates in which such conditions might be available in terms of trucks, off-road vehicles, and off-road terrain driving. It seems that the damping rate can either limit or extend the suspension working space, which is reflected on the span of the relative suspension velocity.

With regards to the suspension stiffness variation, Fig. 11b indicates that the higher harvestable power capacity is obtainable at high stiffness rates. This is related to the remarkable influence of the spring stiffness on the suspension velocity in which the harvestable power strongly correlates to the suspension velocity square. When a softer stiffness is applied, the suspension system might deflect more than the stiffer suspension. However, the relative suspension speed is lower in the case of soft spring than that of the stiff spring. That is why the hard stiffness suspension could reveal higher harvestable power capacity. According to Fig. 11c, it is observed that the tire stiffness variation presented a strong correlation and sensitivity change in terms of the harvestable power content. At higher tire stiffnesses, the tire loses its damping, and the vibration is transferred to the suspension assembly with

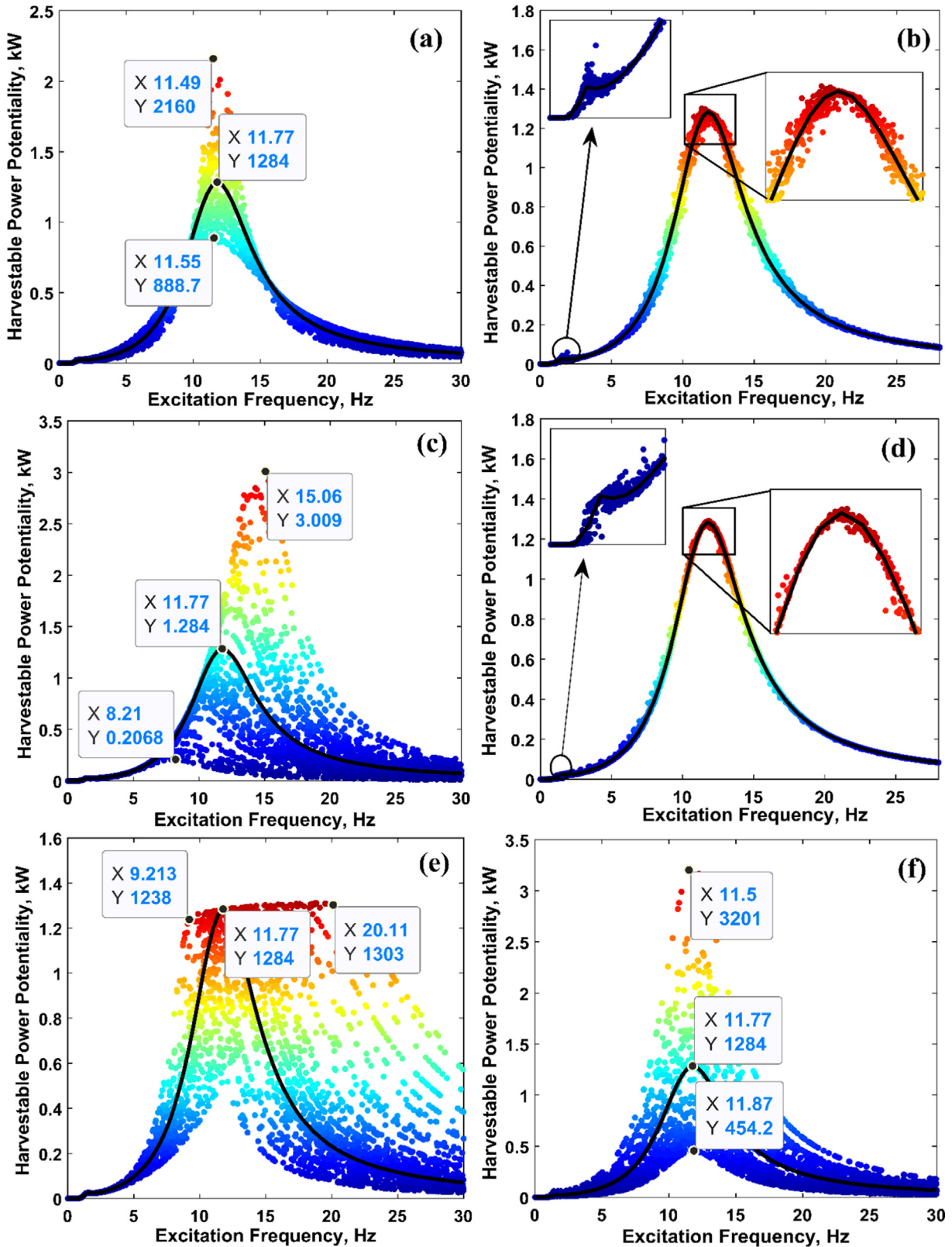


Fig. 11. Bandwidth analysis of the harvestable power magnitude with respect to suspension parameters variation; (a) damping rate variation, (b) spring stiffness variation, (c) tire stiffness variation, (d) sprung mass variation, (e) unsprung mass variation, (f) excitation amplitude variation.

higher density levels making the suspension deflects faster, which resulted in higher harvestable power capacities. In Fig. 11d, when the vehicle body mass increased, the vehicle body resistance against the vibrations increased, which suppresses the vibration

intensities and thereby the relative suspension velocity is suppressed leading to lower kinetic energy dissipation.

The harvesting power is weakly responded to the slighter variation in the wheel mass parameter, as seen in Fig. 11e. The main

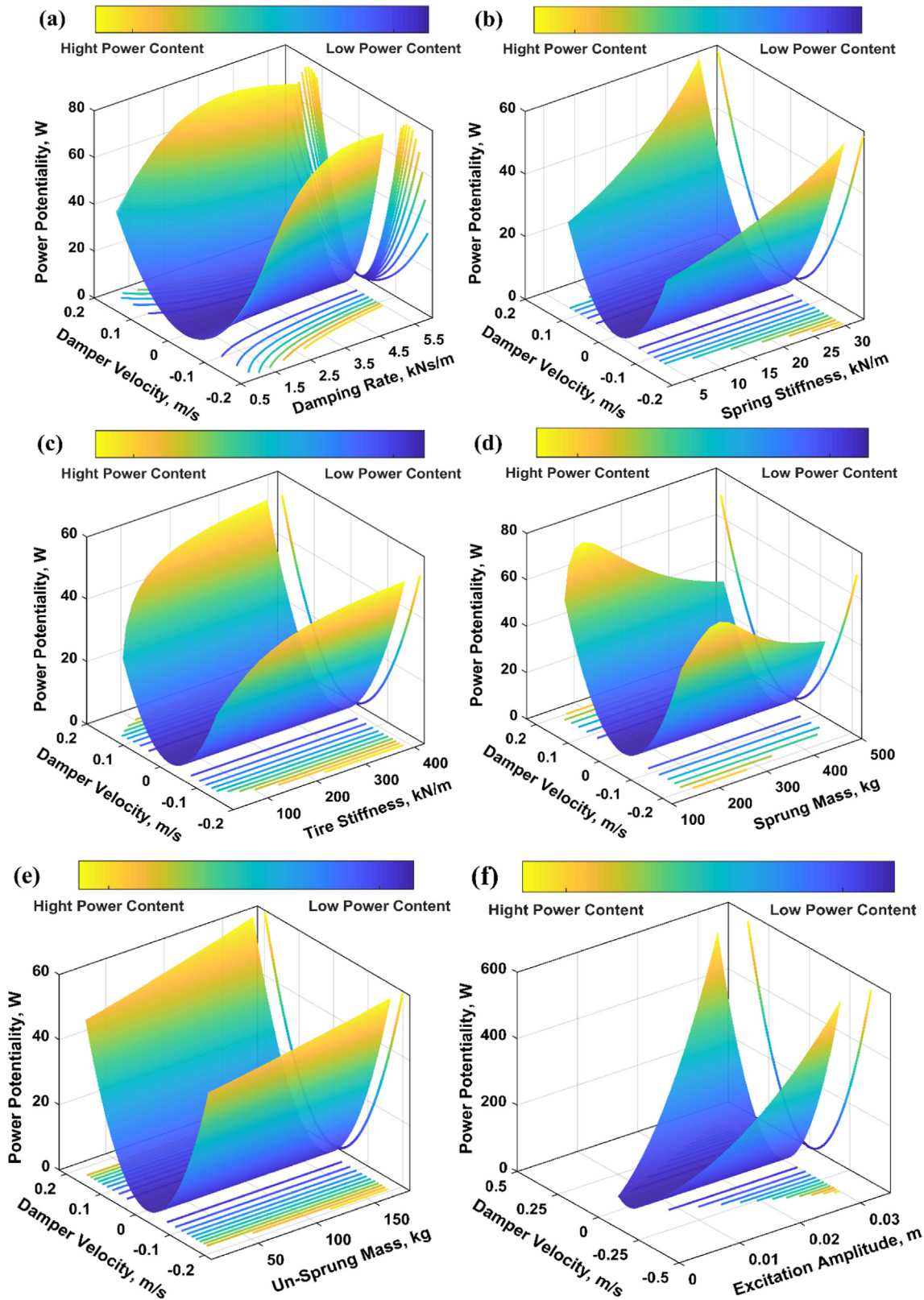


Fig. 12. Harvestable power functioned of the damping velocity with respect to suspension parameters; (a) damping rate variation, (b) spring stiffness variation, (c) tire stiffness variation, (d) sprung mass variation, (e) unsprung mass variation, (f) excitation amplitude variation.

observation here is that the sensitivity change of the harvestable power magnitude correlated weakly to the unsprung mass variation because of the lower influence of the unsprung mass on the suspension velocity. The influence of the excitation amplitude is

then clarified in Fig. 11f. Road elevation significantly enhanced the harvestable power magnitude because the excitation amplitude showed a significantly higher impact on the wheel-body relative movement compared to other suspension parameters. This

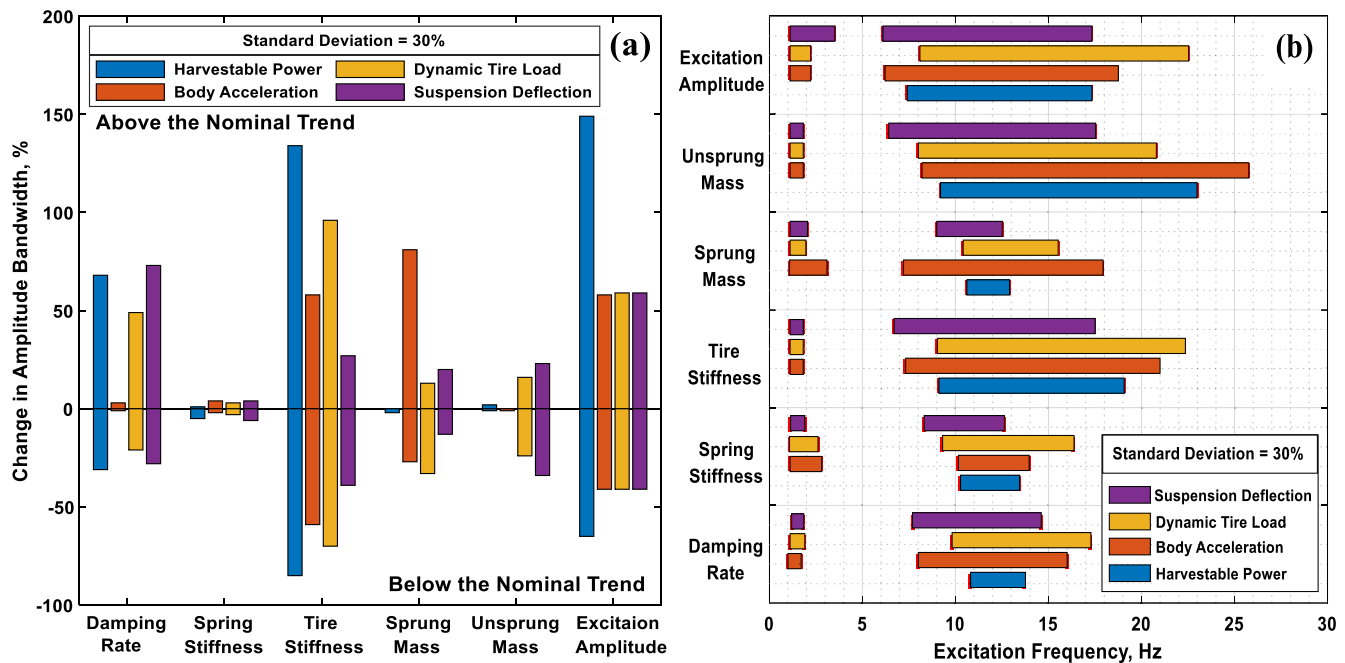


Fig. 13. Conclusion of the bandwidth analysis of the vehicular dynamics and harvestable power magnitudes with respect to suspension parameters variation; (a) sensitivity results of the peak amplitude bandwidth, (b) sensitivity results of the resonant frequency bandwidth.

indicates a higher sensitivity in the harvestable power magnitude respecting the excitation amplitude variation.

In closing, Fig. 12 concludes the bandwidth analysis results, including both the amplitude and the frequency bandwidth in terms of the harvestable power, body acceleration, dynamic tire load, and suspension deflection. Concluding the bandwidth sensitivity results of the harvestable power, it is evident from Fig. 12a that the peak-magnitude of the harvestable power presented higher sensitivity change versus the excitation amplitude, tire stiffness, and the damping rate with a corresponding change in its magnitude band of 149%, 134%, and 68%, respectively. Otherwise, the remaining model parameters, including the spring stiffness and the sprung and unsprung masses, presented a lower influence on the harvestable power magnitude and thereby lower sensitivity change. On the other hand, the ride comfort illustrated higher parametric sensitivity versus the mass of the vehicle body, stiffness coefficient of the tire, and the excitation amplitude. While the damping rate, unsprung mass, and the spring stiffness hardly affect the body acceleration magnitude comparing to other parameters. As for the ground holding response, the dynamic tire load magnitude correlated strongly to the tire stiffness, road excitation amplitude, and the damping coefficient, which contrasts to its correlation to the variation of the spring stiffness, sprung mass and the unsprung mass. In Fig. 12b, the frequency bandwidth analysis of the aforementioned responses versus the suspension parameter variation is given. The harvestable damping power showed a broadened bandwidth with respect to the sprung mass, tire stiffness, and the road excitation amplitude. This is related to the influences of these parameters on both the suspension velocity and resonant frequency and thereby could positively broaden the harvestable power magnitude bandwidth (see Fig. 13).

Conclusions

This paper comprehensively conducted a parametrical bandwidth sensitivity analysis of the vehicular harvestable damping power and suspension dynamics, including body acceleration, dynamic tire load, and suspension deflection. In this manner,

frequency-based Monte Carlo sensitivity simulations were performed using a 2-DOF quarter suspension model with respect to a harmonic excitation with a frequency range of 0–30 Hz and a 30% standard deviation of each suspension parameter based on their nominal values. The bandwidth sensitivity analysis included the effect of the suspension stiffness and damping, tire stiffness, vehicle body, and wheel lump, and the harmonic excitation amplitude. The proposed sensitivity simulations contribute positively regarding conceptualizing an efficient design of a wide broadband energy harvesting damper, which leads to improved harvesting efficiencies in different road conditions.

Given the bandwidth sensitivity results, the amplitude broadband of the peak harvestable power magnitude correlated strongly to road excitation parameters, tire stiffness coefficient, and damping rate, while responded weakly to the sprung and unsprung lump and suspension stiffness. For example, the peak magnitude of the harvestable power presented higher sensitivity change versus the excitation amplitude, tire stiffness, and damping rate, with a corresponding sensitivity change in its amplitude band of 149%, 134%, and 68%, respectively. The road excitation parameters, vehicle speed, and the tire properties could considerably broaden the harvestable damping power, which referees to higher harvestable power potentiality corresponding to the off-road automobiles and heavy trucks. On the second hand, the ride comfort illustrated higher parametric sensitivity versus the vehicle body mass, stiffness coefficient of the tire, and the excitation amplitude, unlike the weak correlation versus the damping rate, unsprung mass, and the spring stiffness. With regards to vehicular road holding, the dynamic tire load correlated strongly to the tire stiffness, road excitation amplitude, and the damping coefficient which contrasts to its correlation to the variation of the suspension stiffness and the wheel and body masses.

Compliance with ethics requirements

This article does not contain any studies with human or animal subjects.

Acknowledgements

The authors would like to express their sincere appreciation to Hubei Key Laboratory of Advanced Technology for Automotive Components for continuous support. The authors also acknowledge the support of the Hubei Collaborative Innovation Center for Automotive Components Technology. The authors also wish to thank the editors and reviewers for their precious time and valuable suggestions and comments.

Funding

This work is financially funded by the National Natural Science Foundation of China (NSFC) (Grant No. 51675391). This contribution is also supported by the 111 Project (Grant No. B17034).

Declaration of Competing Interest

The author(s) declared no potential conflicts of interest with respect to the research, authorship, and/or publication of this article.

References

- [1] Khalil AK, Mubarak AM, Kaseb SA. Road map for renewable energy research and development in Egypt. *J Adv Res* 2010;1:29–38.
- [2] Abdelkareem MAA, Xu L, Ali MKA, Elagouz A, Mi J, Guo S, et al. Vibration energy harvesting in automotive suspension system: a detailed review. *Appl Energy* 2018;229:672–99.
- [3] Xie L, Li J, Li X, Huang L, Cai S. Damping-tunable energy-harvesting vehicle damper with multiple controlled generators: design, modeling and experiments. *Mech Syst Sig Process* 2018;99:859–72.
- [4] Zhu H, Li Y, Shen W, Zhu S. Mechanical and energy-harvesting model for electromagnetic inertial mass dampers. *Mech Syst Sig Process* 2019;120:203–20.
- [5] Zhang Y, Guo K, Wang D, Chen C, Li X. Energy conversion mechanism and regenerative potential of vehicle suspensions. *Energy* 2017;119:961–70.
- [6] Abdelkareem MAA, Xu L, Guo X, Ali MKA, Elagouz A, Hassan MA, et al. Energy harvesting sensitivity analysis and assessment of the potential power and full car dynamics for different road modes. *Mech Syst Sig Process* 2018;110:307–32.
- [7] Abdelkareem MAA, Xu L, Ali MKA, El-Daly A-RBM, Hassan MA, Elagouz A, et al. Analysis of the prospective vibrational energy harvesting of heavy-duty truck suspensions: a simulation approach. *Energy* 2019;173:332–51.
- [8] Chandler D. More power from bumps in the road. *MIT Tech Talk* 2009;53:4.
- [9] Ataei M, Asadi E, Goodarzi A, Khajepour A, Khamesee MB. Multi-objective optimization of a hybrid electromagnetic suspension system for ride comfort, road holding and regenerated power. *J Vib Control* 2017;23:782–93.
- [10] Zhang R, Wang X, John S. A comprehensive review of the techniques on regenerative shock absorber systems. *Energies* 2018;11:1167.
- [11] Xiao H, Wang X, John S. A dimensionless analysis of a 2DOF piezoelectric vibration energy harvester. *Mech Syst Sig Process* 2015;58–59:355–75.
- [12] Lei Z, Brian S, Jurgen S, Yu Z. Design and characterization of an electromagnetic energy harvester for vehicle suspensions. *Smart Mater Struct* 2010;19:045003.
- [13] Ahamed R, Rashid M, Ferdaus M, Yusuf HB. Modelling and performance evaluation of energy harvesting linear magnetorheological (MR) damper. *J Low Freq Noise, Vib Active Control* 2017;36:177–92.
- [14] Satpute NV, Satpute SN, Jugulkar LM. Hybrid electromagnetic shock absorber for energy harvesting in a vehicle suspension. *Proc Inst Mech Eng Part C J Mech Eng Sci.* 2017;231:1500–17.
- [15] Xie L, Li J, Cai S, Li X. Electromagnetic energy-harvesting damper with multiple independently controlled transducers: on-demand damping and optimal energy regeneration. *IEEE/ASME Trans Mechatron* 2017;22:2705–13.
- [16] Mi J, Xu L, Guo S, Meng L, Abdelkareem MAA. Energy harvesting potential comparison study of a novel railway vehicle bogie system with the hydraulic-electromagnetic energy-regenerative shock absorber. In: 2017 Joint Rail Conference: American Society of Mechanical Engineers; 2017. p. V001T07A4–VT07A4.
- [17] Mi J, Xu L, Guo S, Abdelkareem MAA, Meng L, Zuo L. The dimension match and parameters setting of the hydraulic motor for the hydraulic-electromagnetic energy-regenerative shock absorber. *ASME 2017 international design engineering technical conferences and computers and information in engineering conference.* American Society of Mechanical Engineers Digital Collection; 2017.
- [18] Zhu H, Yang J, Zhang Y. Modeling and optimization for pneumatically pitch-interconnected suspensions of a vehicle. *J Sound Vib* 2018;432:290–309.
- [19] Galluzzi R, Xu Y, Amati N, Tonoli A. Optimized design and characterization of motor-pump unit for energy-regenerative shock absorbers. *Appl Energy* 2018;210:16–27.
- [20] Zou J, Guo X, Abdelkareem MAA, Xu L, Zhang J. Modelling and ride analysis of a hydraulic interconnected suspension based on the hydraulic energy regenerative shock absorbers. *Mech Syst Sig Process* 2019;127:345–69.
- [21] Mi J, Xu L, Guo S, Abdelkareem MAA, Meng L. Suspension performance and energy harvesting property study of a novel railway vehicle bogie with the hydraulic-electromagnetic energy-regenerative shock absorber. *SAE paper* 2017-01-14832017.
- [22] Ning D, Sun S, Du H, Li W, Zhang N. Vibration control of an energy regenerative seat suspension with variable external resistance. *Mech Syst Sig Process* 2018;106:94–113.
- [23] Abdelkareem MAA, Xu L, Ali MKA, Hassan MA, Elagouz A, Zou J. On-field measurements of the dissipated vibrational power of an SUV car traditional viscous shock absorber. *ASME 2018 International design engineering technical conferences and computers and information in engineering conference.* American Society of Mechanical Engineers Digital Collection; 2018.
- [24] Zuo L, Zhang P-S. Energy harvesting, ride comfort, and road handling of regenerative vehicle suspensions. *J Vib Acoust* 2013;135:011002.
- [25] Zhao Z, Wang T, Shi J, Zhang B, Zhang R, Li M, et al. Analysis and application of the piezoelectric energy harvester on light electric logistics vehicle suspension systems. *Energy Sci Eng* 2019;7:2741–55.
- [26] Abdelkareem MA, Kaldas MM, Kamal Ahmed Ali M, Xu L. Analysis of the energy harvesting potential-based suspension for truck semi-trailer. *Proc Inst Mech Eng Part D J Automob Eng* 2019;233:2955–69.
- [27] Riese C, Stump O, Gauterin F. Investigation of the energy recuperation potential of the damper system for a compact class passenger car. *Int J Veh Des* 2017;74:281–303.
- [28] Taghavifar H, Rakheja S. Parametric analysis of the potential of energy harvesting from commercial vehicle suspension system. *Proc Inst Mech Eng Part D J Automob Eng* 2019;233:2687–700.
- [29] Zhang R, Wang X, Liu Z. A novel regenerative shock absorber with a speed doubling mechanism and its Monte Carlo simulation. *J Sound Vib* 2018;417:260–76.
- [30] Zhang R, Wang X, Al Shami E, John S, Zuo L, Wang CH. A novel indirect-drive regenerative shock absorber for energy harvesting and comparison with a conventional direct-drive regenerative shock absorber. *Appl Energy* 2018;229:111–27.
- [31] Sattar AM, Raslan YM. Predicting morphological changes ds new Naga-Hammadi barrage for extreme Nile flood flows: a Monte Carlo analysis. *J Adv Res* 2014;5:97–107.
- [32] Liu B, Xu L, Zhao Z, Abdelkareem MAA, Zou J, Yu J. Modeling and simulation of a displacement controllable active suspension system. In *ASME 2018 International design engineering technical conferences and computers and information in engineering conference.* American Society of Mechanical Engineers Digital Collection; 2018.
- [33] Abdelkareem MAA, Makrahy MM, Abd-El-Tawwab AM, EL-Razaz A, Ali MKA, Moheyeldin M. An analytical study of the performance indices of articulated truck semi-trailer during three different cases to improve the driver comfort. *Proc Inst Mech Eng Part K J Multi-body Dyn* 2018;232:84–102.
- [34] Nagarkar MP, Patil GJV, Patil RNZ. Optimization of nonlinear quarter car suspension-seat-driver model. *J Adv Res* 2016;7:991–1007.
- [35] Abdelkareem MAA, Xu L, Zou J, Ali MKA, Essa FA, Elagouz A, et al. energy-harvesting potential and vehicle dynamics conflict analysis under harmonic and random road excitations. *SAE Int* 2018.
- [36] Zhu Z, Xu L, Abdelkareem MAA, Zou J, Mi J. Design and simulation analysis of vibration energy harvesting system based on ADAMS. *ASME 2019 International design engineering technical conferences and computers and information in engineering conference.* 2019.